SHORT REPORT

A systematic survey of conformational states in β1 and β4 integrins using negative-stain electron microscopy

Naoyuki Miyazaki, Kenji Iwasaki* and Junichi Takagi*

ABSTRACT

Structural analyses of β2 and β3 integrins have revealed that they generally assume a compact bent conformation in the resting state and undergo a global conformational transition involving extension during upregulation of ligand affinity, collectively called the 'switchblade model'. This hypothesis, however, has not been extensively tested for other classes of integrins. We prepared a set of recombinant integrin ectodomain fragments including αvβ3, α2β1, α3β1, α5β1, α6β1 and α6β4, and used negative-stain electron microscopy to examine their structures under various conditions. In contrast to αvβ3 integrin, which exhibited a severely bent conformation in low-affinity 5 mM Ca^{2+} conditions, all β1 integrin heterodimers displayed a mixed population of half-bent to fully extended conformations. Moreover, they did not undergo significant conformational change upon activation by Mn^{2+}. Integrin α6β4 was even more resistant to conformational regulation, showing a completely extended structure regardless of the buffer conditions. These results suggest that the mechanisms of conformational regulation of integrins are more diverse and complex than previously thought, requiring more experimental scrutiny for each integrin subfamily member.

KEY WORDS: Laminin, Integrin, Electron microscopy, Conformational change

INTRODUCTION

Integrins are a family of cell adhesion receptors that mediate cell-cell and cell-extracellular matrix interactions and govern migration and anchorage for almost all kinds of cells. Mammalian genomes contain up to 18 α- and 8 β-subunits that combine to form 24 different heterodimers, each of which has an apparently unique ligand-binding profile and biological function (Humphries, 2000; Hynes, 2002). Crystal structures of the full-length extracellular domain have been determined for three integrins (αVβ3, Xiong et al., 2001, 2002; αIIbβ3, Zhu et al., 2008; and αXβ2, Xie et al., 2010; Sen et al., 2013) among the 24 dimers to date. Although these integrins were all crystallized in a highly compact and counterintuitive 'bent' conformation, subsequent electron microscopy (EM) studies identified very different and much more intuitive 'extended' conformations in addition to the bent conformation, especially when integrins were activated (Nishida et al., 2006; Takagi et al., 2002). As this large conformational

change coincided with the change in affinity and/or ligand binding states of integrins, a hypothesis called the 'switchblade' (or jack-knife) model was proposed to describe the mechanism for the bidirectional signal transduction (outside-in and inside-out signaling) across a cytoplasmic membrane (Takagi et al., 2002; Takagi and Springer, 2002). The description of the conformational states has been refined by numerous structural studies and it is now generally accepted that integrin can assume three distinct conformations: a bent integrin with a closed headpiece, an extended integrin with a closed headpiece and an extended integrin with an open headpiece, where the former two represent integrins with low ligand affinity (Luo and Springer, 2006).

In β2 and β3 integrins, experimental data from a range of sources including EM, biophysical, immunochemical and computational studies overwhelmingly support the close linkage between affinity state modulation and the structural rearrangements in overall ectodomain and headpiece conformations (Xie et al., 2004; Rocco et al., 2008; Chen et al., 2010, 2011; Nishida et al., 2006; Takagi et al., 2002). Furthermore, in addition to the studies using soluble ectodomain truncations of integrins, detergent-solubilized intact integrins or intact integrins embedded in phospholipid nanodiscs support the structural rearrangement model during activation (Iwasaki et al., 2005; Eng et al., 2011; Xu et al., 2016; Ye et al., 2010). Considering the high degree of sequence conservation among 8 integrin β-subunits and the fact that many β-subunits share identical α-subunits, it was reasonable to expect that the switchblade model applies to all integrin subfamily members. However, recent EM-based studies suggested that this simple assumption may not hold true, at least for some integrins. For example, it was shown that αVβ8 integrin assumed a constitutively extended conformation, regardless of the affinity states toward its physiological ligand, latent TGF-β (Wang et al., 2017; Minagawa et al., 2014). Furthermore, Springer and colleagues reported that the α5β1 integrin ectodomain rarely assumed the acutely bent conformation even in its resting (i.e. low-affinity) condition, and its affinity state was strongly correlated with head-opening but not with global extension (Su et al., 2016). Therefore, it is becoming clear that the link between the global conformational change and the ligand affinity state for a given integrin subtype must be more carefully examined for individual integrins. In particular, elucidation of the regulatory mechanisms for laminin-binding integrins that have evaded structural scrutiny to date is urgently needed, because they comprise ancient and fundamental integrin classes responsible for cell attachment to the basement membrane, which is crucial for all multicellular animals (Hynes and Zhao, 2000; Hutter et al., 2000).

In the current work, we obtained negative-stain EM images of the ectodomain fragment of β1 and β4 integrins, including fibronectin-binding (α5β1), laminin-binding (α3β1, α6β1 and α6β4) and collagen-binding (α2β1) integrins, in both resting (i.e. in 5 mM Ca^{2+}) and activating (i.e. in 1 mM Mn^{2+}) conditions, and made side-by-side comparisons with images of the

well-studied αVβ3 integrin. In contrast to the αVβ3 integrin, which primarily assumes a bent conformation in the resting condition, all β1 and β4 integrins exhibited a range of conformations with the majority of the particles showing overall extended conformation. Surprisingly, they do not undergo either local (i.e. head opening) or global (i.e. extension) conformational change upon the shift to a more activating condition, suggesting that the affinity upregulation of these integrins can occur in the absence of obvious conformational change that can be detected by low-resolution EM analysis.

RESULTS AND DISCUSSION
Ligand binding activities of β1 and β4 integrins
Soluble extracellular fragments of integrins each containing a releasable C-terminal clasp (Fig. 1A) were purified as described in the Materials and Methods. The α- and β-subunits were linked by a disulfide-bonded clasp and migrated as a single band in the SDS-PAGE under nonreducing conditions (TEV− lanes in Fig. 1B). By contrast, they were separated into two bands after TEV protease treatment (TEV+ lanes in Fig. 1B). Thus, it was confirmed that all purified integrin heterodimers were linked via

a disulfide-bonded clasp at the C-terminal, which can be released (or 'unclasped') by TEV protease treatment. These integrins were subjected to the following experiments (ligand binding assay and structural analysis by electron microscopy). As reported previously (Takagi et al., 2002), binding of αVβ3 integrin to its ligand was negligible in the presence of 5 mM Ca^{2+} but was upregulated 4- to 5-fold over the background (i.e. BSA control) level in the presence of 1 mM Mn^{2+} in both clasped and unclasped conditions (Fig. 1C, far left panel), indicating that the 5 mM Ca^{2+} and the 1 mM Mn^{2+} conditions correspond to the low- and high-affinity states, respectively. We deliberately employed a non-physiologically high concentration of Ca^{2+} (5 mM) to push the equilibrium toward the low-affinity state by saturating the βI domain ADMIDAS with Ca^{2+}, which has been reported to have negative regulatory function (Mould et al., 2003). The ADMIDAS-bound Ca^{2+} is believed to stabilize the low-affinity conformation of the ligand-engaging MIDAS metal through its preference toward pentagonal bipyramidal over octahedral coordination geometry (Xia and Springer, 2014). When another RGD-dependent integrin α5β1 was subjected to the same assay using immobilized fibronectin, the results were essentially the same, although the overall binding signal was much higher
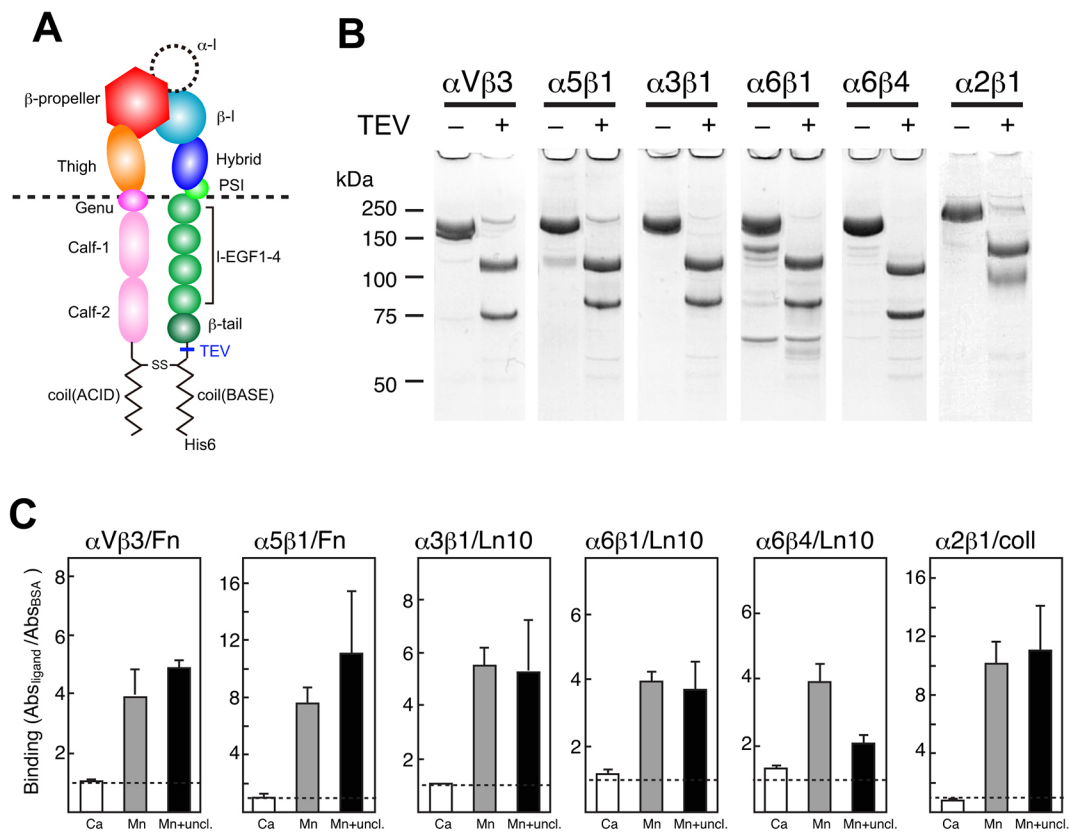

Fig. 1. Recombinant integrin ectodomain proteins. (A) Domain organization of the integrin ectodomain constructs used in this study. Each domain is color-coded and schematically drawn, together with the disulfide-bonded coiled-coil 'clasp' fused at the C-terminus. The approximate position of the hinge during the global bending motion is indicated by a horizontal dashed line. (B) SDS-PAGE analysis of recombinant integrins. Purified recombinant integrin samples were either unclasped by TEV protease (+) or left untreated (−) and subjected to nonreducing SDS-PAGE using 10% gel and stained with Coomassie Brilliant Blue. Note that all intact integrin heterodimers migrate as a single band of 200-250 kDa but show two bands corresponding to α (∼120-150 kDa) and β (80-100 kDa) subunits after the removal of disulfide-bonded C-terminal clasp by the TEV protease treatment. Difference in the apparent size of the β1 band of the α2β1 sample compared with other β1 integrins is consistent with the different glycosylation capacities of the cell line used for protein production. (C) Ligand binding activities of various integrins. Binding of integrins to their respective primary ligand (laminin-10 for α3β1, α6β1 and α6β4; fibronectin for α5β1 and αVβ3; type I collagen for α2β1) was evaluated by a solid-phase binding assay under three different conditions. Open bars represent intact integrin in the presence of 5 mM Ca^{2+}; gray bars show intact integrin in the presence of 1 mM Mn^{2+}; black bars show unclasped integrin in the presence of 1 mM Mn^{2+}. Binding is expressed as the ratio of absorbance values obtained with the ligand-coated wells relative to that with BSA control wells, where ratio=1 (dashed lines) means that there is no specific binding to the ligand. Data represent mean±s.d. from three independent experiments.

(Fig. 1C, second panel). We then examined the ligand binding ability of all other non-RGD integrins toward laminin-10 (for integrins α3β1, α6β1 and α6β4) or type I collagen (for α2β1) using the same assay conditions. As shown in Fig. 1C, they all showed similar ligand binding to αVβ3 integrin; binding was negligible in 5 mM Ca^{2+} but high ligand binding activities were observed in the presence of Mn^{2+}. Importantly, the extent of ligand binding under Mn^{2+} conditions for each integrin was almost the same irrespective of the state of the C-terminal clasp (clasped or unclasped), except for α6β4 integrin. In the case of the α6β4 integrin, unclasping resulted in diminished binding to laminin-10, although there was still clear binding above background levels and above the level seen in Ca^{2+} conditions. From these results, we conclude that 5 mM Ca^{2+} and 1 mM Mn^{2+} can be used as representative conditions to induce low- and high-affinity states, respectively, for all integrin ectodomain fragments used here.

EM imaging of β1 and β4 integrins

Having established the experimental conditions to maintain various integrins in the low- and high-affinity states, we turned to negative-stain EM imaging to visualize the conformation of each integrin under both conditions. To this end, integrin samples were loaded onto a gel filtration column equilibrated with a buffer containing 5 mM Ca^{2+} (low-affinity state) or 1 mM Mn^{2+} (high-affinity state) and the monodisperse peak fraction containing the heterodimeric integrin ectodomain was used to make EM grids. We also included one more condition, where 1 mM Mg^{2+} was added to 5 mM Ca^{2+} buffer. Data were collected for all six integrins under four different conditions (clasped/5 mM Ca^{2+}, clasped/5 mM Ca^{2+}+1 mM Mg^{2+}, clasped/1 mM Mn^{2+} and unclasped/1 mM Mn^{2+}). As can be seen in the representative raw EM image (Fig. S1), all samples showed well-dispersed individual particles that allowed efficient image analysis. From the EM images obtained, ~1000 particles in each condition were boxed out, and they were averaged after classification into 20 classes. We used αVβ3 integrin as a reference, because this is the most extensively studied integrin by multiple groups using EM analysis. As expected, nearly all αVβ3 particles exhibited a highly bent conformation in 5 mM Ca^{2+} regardless of the additional presence of Mg^{2+}. In the Mn^{2+} condition, a large majority changed their shape and showed a completely extended and open conformation consistent with the 'switchblade model' (Fig. S2A). The behavior of α5β1 integrin was quite different from that of αVβ3, however, because it rarely assumed the acutely bent conformation in the low-affinity condition but rather exhibited varying shapes, with partly to fully extended conformations being predominant (Fig. 2A and Fig. S2B). In fact, this result is essentially the same as that reported by Springer and colleagues (Su et al., 2016). The authors showed that only a fraction of EM class averages of ligand-unbound and clasped α5β1 ectodomain fragment appeared as the acutely bent form in a buffer containing 1 mM Ca^{2+} and 1 mM Mg^{2+}. More importantly, the shape distribution of α5β1 particles did not change when the high-affinity condition (i.e. 1 mM Mn^{2+}) was employed (Fig. 2B and Fig. S2B), suggesting the lack of a strong correlation between the affinity state and the global conformation in α5β1. Despite high variability of the particle shapes of α5β1 in the EM images, most 2D class averages showed clear and distinctive features that helped us to assign each chain or domain present in the construct (Fig. 1A) into the densities, enabling us to interpret the 3D structure (Fig. 2C) and to classify particles according to their global conformation (see below).

We next performed similar EM imaging on laminin- and collagen-binding integrins that had escaped structural scrutiny until now, namely α3β1, α6β1, α6β4 and α2β1. In general, the results were

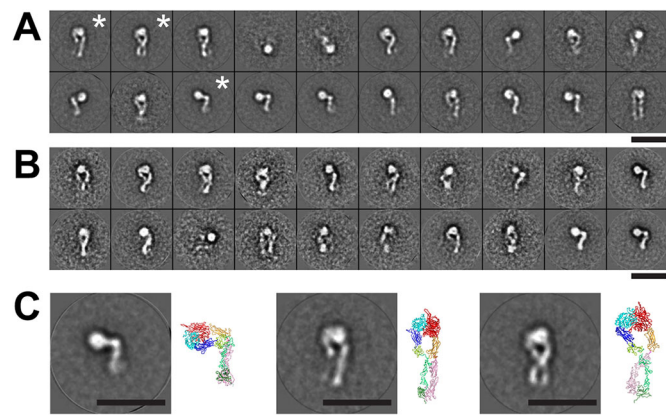**Fig. 2. Projection averages of negatively stained α5β1 integrin.** All 20 2D class averages obtained from the EM images of clasped α5β1 integrin in the presence of 5 mM Ca^{2+} (A) or 1 mM Mn^{2+} (B). (C) Three particularly well-resolved class averages with different bending angles from A (marked with asterisks) are enlarged and shown alongside the best-matching structural models (color-coded as in Fig. 1A). Bars: 25 nm.

almost the same as that of α5β1 integrin (Fig. 3 and Fig. S2C-F). No severely bent conformation was observed for any of these integrins, even in the low-affinity state, and the majority of the class averages exhibited an overall extended conformation. Furthermore, the conformational distribution seen in the Mn^{2+}-activated condition for the three laminin-binding integrins was indistinguishable from that in the Ca^{2+} or Ca^{2+}/Mg^{2+} condition, regardless of the presence of the C-terminal clasp (Fig. 3 and Fig. S2C-E). In particular, α6β4 integrin almost always assumed the completely extended structure regardless of the condition (Fig. S2E), suggesting that it is mostly refractory to conformational regulation. In the case of α2β1 integrin, there is an additional I (A) domain in the α-subunit, which was clearly visible at the top of the molecule in the class-averaged images (Fig. S2F). Although it shared the same trend with laminin-binding integrins of having the overall extended conformation in both low- and high-affinity conditions, there was a clear local conformational change upon addition of Mn^{2+}, corresponding to head opening (i.e. the swing-out of the hybrid domain of the β-subunit). As the αI domain functions as an internal ligand to the β-subunit (Sen et al., 2013), Mn^{2+}-treated α2β1 would represent the 'active and liganded' state rather than the 'active and non-liganded' state, as in the case of all other integrins lacking domain I. Therefore, these results are highly consistent with the notion that the β-hybrid swing is coupled to ligand binding rather than the affinity state of integrin (Su et al., 2016).

Conformational spectra of β1 and β4 integrins

The individual class average was categorized into five groups based on their shape (Fig. S2), and the prevalence of each group was calculated from the numerical values obtained during single-particle analysis. As none of the integrins showed a significant difference in the conformational distribution between Ca^{2+} and Ca^{2+}/Mg^{2+} conditions, as well as between clasped/Mn^{2+} and unclasped/Mn^{2+} samples, we will focus on the comparison between the clasped/Ca^{2+} and clasped/Mn^{2+} conditions. The population prevalence determined as above can be regarded as the approximate 'conformational distribution spectra' for each integrin or condition (Fig. 3). It is evident from this analysis that all examined β1 and β4 integrins prefer the extended conformation (colored in yellow, orange or magenta) over bent conformation (blue and green) under the Ca^{2+}-induced low-affinity condition, and rarely assumed the severely bent conformation (blue) that is
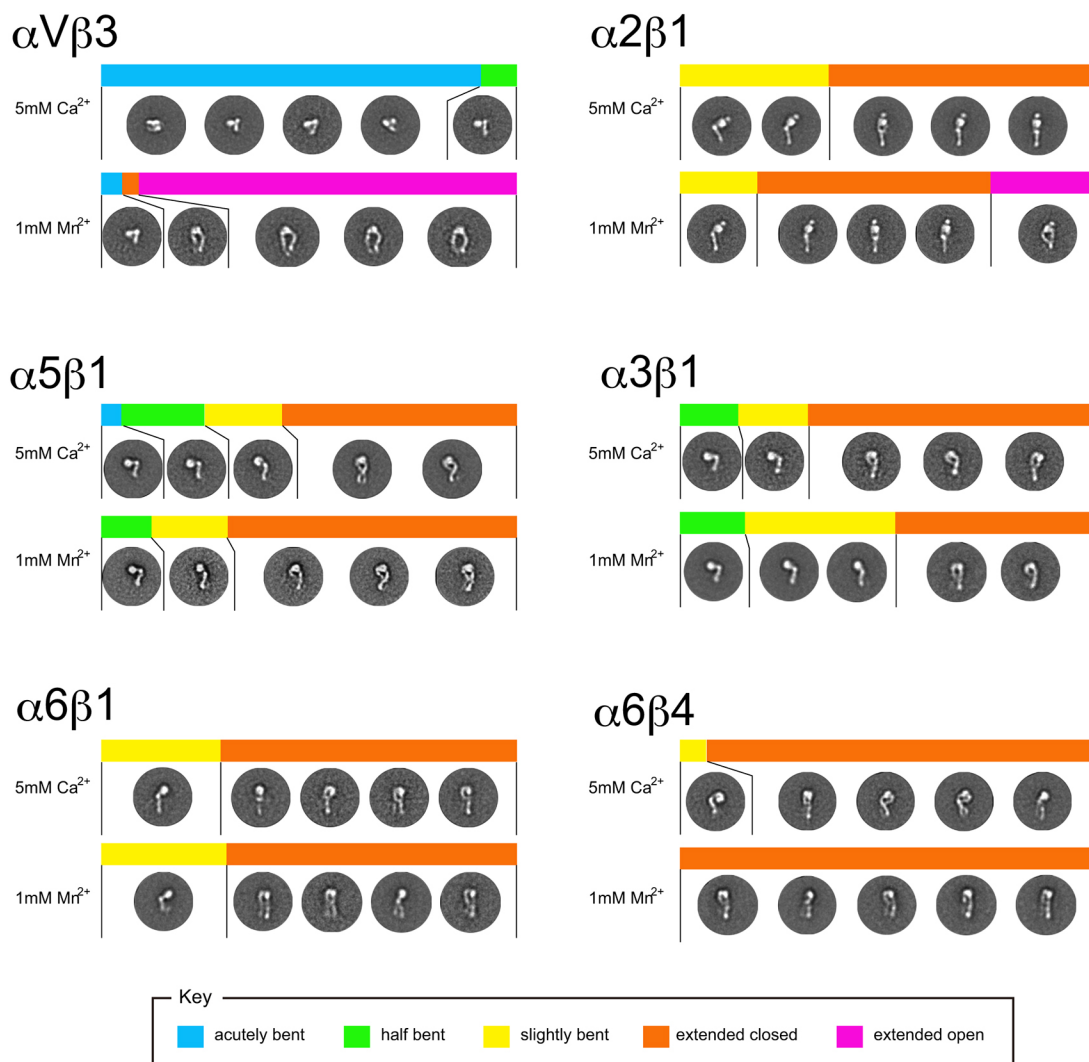
3

Fig. 3. The conformational distribution spectra for various integrins under low-affinity (5 mM Ca²⁺) and high-affinity (1 mM Mn²⁺) conditions.
The colored bar graphs represent percentage distribution of five conformational groups within the 2D class averages obtained for each dataset. The five groups include: (1) compact integrin with a bending angle <90° (acutely bent, blue); (2) integrin with a bending angle obtained between 90° and 120° (half bent, green); (3) integrin with a bending angle over 120° (slightly bent, yellow); (4) integrin showing fully extended conformation with closed headpiece (extended closed, orange); and (5) integrin showing fully extended conformation with open headpiece (extended open, magenta). Representative 2D averages are shown below the bar graph. For the original full class average gallery and particle number information, see Fig. S2.

strongly favored by the well-studied β2 and β3 integrins. Furthermore, there seems to be no or very limited coupling between the affinity state and the global conformation of these integrins, because nearly identical conformational distributions were obtained for the Ca²⁺ and Mn²⁺ conditions. We are thus inclined to think that the switchblade model is not applicable to most if not all β1 and β4 integrins, at least as an affinity regulation mechanism. However, data must be interpreted in a careful manner to avoid overgeneralization, as the current study used only the soluble integrin ectodomain fragments. In addition, as the direct structural analysis is only possible with isolated integrin preparations, it is difficult to know the true conformational spectrum on the cell surface. For example, Springer and colleagues estimate that more than 98% of the α5β1 molecule on K562 cells are in the bent form (Li et al., 2017). It is possible that certain mechanisms exist on the cell surface to stabilize a bent conformation, at least for α5β1. Nevertheless, our data indicate that the ectodomain portions of β1 and β4 integrins lack the

intrinsic property of rearrangement upon affinity manipulation by divalent cations.

Unlike the integrins present on circulating blood cells, including αIIbβ3, αVβ3, αXβ2 and αLβ2, which have to bind ligands during transient encounters, laminin-binding integrins (α3β1, α6β1, α7β1 and α6β4) and collagen-binding integrins (α1β1, α2β1, α10β1 and α11β1) on stationary cells generally have ample time to establish firm adhesion due to continuous contact with the extracellular components, and may not need mechanisms of rapid affinity upregulation. Thus the rapid 'switchblade' activation, in a strict sense, may only be applicable to those integrins on blood cells that emerged at a relatively late evolutionary point after the acquisition of the vascular system. Although there is strong coupling between ligand binding and global and local conformation of a wide variety of integrins (Takagi et al., 2002; Nishida et al., 2006; Chen et al., 2010, 2011; Rocco et al., 2008; Xie et al., 2004; Su et al., 2016), we do not have direct evidence that such coupling is applicable to laminin-binding integrins. This is mainly due to the limited

structural information available for the laminin-integrin interaction (Takizawa et al., 2017). We predict that further structural analysis as well as development of biochemical tools, such as high-affinity laminin mimetic ligands to probe the interaction between laminin and integrin, will be essential to increase our understanding about this fundamental and ancient cell-matrix interaction event.

MATERIALS AND METHODS

Preparation of soluble ectodomain of various integrins

Soluble integrin heterodimers were constructed using a strategy described previously (Takagi et al., 2001). Briefly, the expression constructs for the α-subunits contained an extracellular portion of each α-chain (residues 1-1103 for α2, residues 1-957 for α3, residues 1-950 for α5, residues 1-988 for α6, and residues 1-960 for αV) followed by a 30-residue ACID-Cys peptide. Constructs for β-subunits contained an extracellular portion of each β-chain (residues 1-708 for β1, residues 1-691 for β3 and residues 1-683 for β4) followed by a TEV protease recognition sequence, a 30-residue BASE-Cys peptide and a hexahistidine tag. When combined, the C-terminal ACID-Cys and BASE-Cys segments form the inter-subunit disulfide-bridged α-helical coiled-coil ('clasp') that can be released by a treatment with TEV protease (Takagi et al., 2002). The general architecture of recombinant soluble integrin heterodimers is shown in Fig. 1A. Appropriate combinations of α- and β-constructs were co-transfected into either CHO lec 3.2.8.1 cells (for α3β1, α5β1, α6β1, α6β4 and αVβ3) (a gift from Pamela Stanley, Albert Einstein College of Medicine, New York, USA) or HEK293-EBNA cells (for α2β1) (Thermo Fisher Scientific) to establish stable cell lines. Recombinant integrins were purified from the culture supernatants by an immunoaffinity chromatography using anti-coiled-coil antibody 2H11 (a gift from Ellis Reinherz, Dana Farber Cancer Institute, Boston, USA; Chang et al., 1994), followed by a gel filtration on a Superdex 200 HR column (1.6×60 cm, GE Healthcare) equilibrated with 20 mM Tris-HCl, 150 mM NaCl, pH 7.5 (TBS) containing 1 mM $CaCl_2$, 1 mM $MgCl_2$. The peak fraction was concentrated to ∼1 mg/ml and stored at −80°C until used. To obtain unclasped integrins, purified clasped integrins were treated with recombinant TEV protease at 20°C for 16 h.

Ligand binding assay

Ligand binding assays were performed as described previously (Nishiuchi et al., 2006). Briefly, solutions of recombinant laminin-10 (20 µg/ml, a gift from Kiyotoshi Sekiguchi, Institute for Protein Research, Osaka Japan), bovine fibronectin (10 µg/ml, Sigma), or rat type I collagen (10 µg/ml, Sigma) in TBS were used to coat 96-well polyvinylchloride microtiter plates (Nunc, Maxisorp) by an overnight incubation at 4°C. Coating with bovine serum albumin (BSA) was used to determine the background values of unspecific binding. After a 1 h blocking step (1% BSA in TBS), various integrins were added to the plates at 25 µg/ml (α6β4) or 1 µg/ml (all other integrins) and allowed to bind the absorbed ligand for 4 h at room temperature. The reaction mixture contained either 5 mM $CaCl_2$ (low-affinity condition) or 1 mM $MnCl_2$ (high-affinity condition). The plates were washed with TBS containing 1 mM $MnCl_2$ and the bound integrins were quantified by an enzyme-linked immunosorbent assay using biotinylated rabbit anti-clasp (ACID/BASE coiled-coil) antibody (made in-house; Nishiuchi et al., 2006) and HRP-conjugated streptavidin (SA-5004, VECTOR Laboratories).

Electron microscopy and image analysis procedures

Approximately 10 µg of each purified integrin was subjected to an additional gel filtration on a Superdex 200 HR column with 50 mM Tris-HCl, 150 mM NaCl, pH 7.5 containing 5 mM $CaCl_2$ or 1 mM $MnCl_2$. The samples after the gel filtration were immediately absorbed to glow-discharged carbon-coated copper grids. Samples were negatively stained with 2.5% (w/v) uranyl acetate and examined under an electron microscope (H9500SD; Hitachi, Japan) operated at 200 kV and a nominal magnification of ×80,000. Tobacco mosaic virus was added to specimens to control the depth of staining, which was also used for calibrating magnification (large rod-like objects in Fig. S1). Images were recorded on a 2048×2048 CCD camera (TVIPS, Gauting, Germany). Single-particle

analysis, including particle selection and 2D classification and averaging, was performed using the EMAN software suite (Ludtke et al., 1999) and IMAGIC (van Heel et al., 1996). Particles were selected from individual frames (with an effective pixel size of 0.21 nm) using the program Boxer in the EMAN software suite. The particle images were rotationally and translationally aligned by a multi-reference alignment procedure and subjected to multivariate statistical analysis specifying 20 classes using the IMAGIC program.

References

Chang, H. C., Bao, Z., Yao, Y., Tse, A. G., Goyarts, E. C., Madsen, M., Kawasaki, E., Brauer, P. P., Sacchettini, J. C. and Nathenson, S. G. (1994). A general method for facilitating heterodimeric pairing between two proteins: application to expression of alpha and beta T-cell receptor extracellular segments. *Proc. Natl. Acad. Sci. USA* **91**, 11408-11412.

Chen, X., Xie, C., Nishida, N., Li, Z., Walz, T. and Springer, T. A. (2010). Requirement of open headpiece conformation for activation of leukocyte integrin alphaXbeta2. *Proc. Natl. Acad. Sci. USA* **107**, 14727-14732.

Chen, W., Lou, J., Hsin, J., Schulten, K., Harvey, S. C. and Zhu, C. (2011). Molecular dynamics simulations of forced unbending of integrin alpha(v)beta(3). *PLoS Comput. Biol.* **7**, e1001086.

Eng, E. T., Smagghe, B. J., Walz, T. and Springer, T. A. (2011). Intact alpha(IIb)beta(3) integrin is extended after activation as measured by solution x-ray scattering and electron microscopy. *J. Biol. Chem.* **286**, 35218-35226.

Humphries, M. J. (2000). Integrin structure. *Biochem. Soc. Trans.* **28**, 311-339.

Hutter, H., Vogel, B. E., Plenefisch, J. D., Norris, C. R., Proenca, R. B., Spieth, J., Guo, C., Mastwal, S., Zhu, X., Scheel, J. et al. (2000). Conservation and novelty in the evolution of cell adhesion and extracellular matrix genes. *Science* **287**, 989-994.

Hynes, R. O. (2002). Integrins: bidirectional, allosteric signaling machines. *Cell* **110**, 673-687.

Hynes, R. O. and Zhao, Q. (2000). The evolution of cell adhesion. *J. Cell Biol.* **150**, F89-F96.

Iwasaki, K., Mitsuoka, K., Fujiyoshi, Y., Fujisawa, Y., Kikuchi, M., Sekiguchi, K. and Yamada, T. (2005). Electron tomography reveals diverse conformations of integrin alphaIIbbeta3 in the active state. *J. Struct. Biol.* **150**, 259-267.

Li, J., Su, Y., Xia, W., Qin, Y., Humphries, M. J., Vestweber, D., Cabañas, C., Lu, C. and Springer, T. A. (2017). Conformational equilibria and intrinsic affinities define integrin activation. *EMBO J.* **36**, 629-645.

Ludtke, S. J., Baldwin, P. R. and Chiu, W. (1999). EMAN: semiautomated software for high-resolution single-particle reconstructions. *J. Struct. Biol.* **128**, 82-97.

Luo, B.-H. and Springer, T. A. (2006). Integrin structures and conformational signaling. *Curr. Opin. Cell Biol.* **18**, 579-586.

Minagawa, S., Lou, J., Seed, R. I., Cormier, A., Wu, S., Cheng, Y., Murray, L., Tsui, P., Connor, J., Herbst, R. et al. (2014). Selective targeting of TGF-beta activation to treat fibroinflammatory airway disease. *Sci. Transl. Med.* **6**, 241ra79.

Mould, A. P., Barton, S. J., Askari, J. A., Craig, S. E. and Humphries, M. J. (2003). Role of ADMIDAS cation-binding site in ligand recognition by integrin alpha 5 beta 1. *J. Biol. Chem.* **278**, 51622-51629.

Nishida, N., Xie, C., Shimaoka, M., Cheng, Y., Walz, T. and Springer, T. A. (2006). Activation of leukocyte beta2 integrins by conversion from bent to extended conformations. *Immunity* **25**, 583-594.

Nishiuchi, R., Takagi, J., Hayashi, M., Ido, H., Yagi, Y., Sanzen, N., Tsuji, T., Yamada, M. and Sekiguchi, K. (2006). Ligand-binding specificities of laminin-binding integrins: a comprehensive survey of laminin-integrin interactions using recombinant alpha3beta1, alpha6beta1, alpha7beta1 and alpha6beta4 integrins. *Matrix Biol.* **25**, 189-197.

Rocco, M., Rosano, C., Weisel, J. W., Horita, D. A. and Hantgan, R. R. (2008). Integrin conformational regulation: uncoupling extension/tail separation from changes in the head region by a multiresolution approach. *Structure* **16**, 954-964.

Sen, M., Yuki, K. and Springer, T. A. (2013). An internal ligand-bound, metastable state of a leukocyte integrin, alpha(X)beta(2). *J. Cell Biol.* **203**, 629-642.

Su, Y., Xia, W., Li, J., Walz, T., Humphries, M. J., Vestweber, D., Cabañs, C., Lu, C. and Springer, T. A. (2016). Relating conformation to function in integrin alpha5beta1. *Proc. Nat.l Acad. Sci. USA* **113**, E3872-E3881.

Takagi, J. and Springer, T. A. (2002). Integrin activation and structural rearrangement. *Immunological Rev.* **186**, 141-163.

Takagi, J., Erickson, H. P. and Springer, T. A. (2001). C-terminal opening mimics "inside-out" activation of integrin a5b1. *Nature Struct. Biol.* **8**, 412-416.

Takagi, J., Petre, B. M., Walz, T. and Springer, T. A. (2002). Global conformational rearrangements in integrin extracellular domains in outside-in and inside-out signaling. *Cell* **110**, 599-611.

Takizawa, M., Arimori, T., Taniguchi, Y., Kitago, Y., Yamashita, E., Takagi, J. and Sekiguchi, K. (2017). Mechanistic basis for the recognition of laminin-511 by alpha6beta1 integrin. *Sci. Adv.* **3**, e1701497.

Van Heel, M., Harauz, G., Orlova, E. V., Schmidt, R. and Schatz, M. (1996). A new generation of the IMAGIC image processing system. *J. Struct. Biol.* **116**, 17-24.

Wang, J., Dong, X., Zhao, B., Li, J., Lu, C. and Springer, T. A. (2017). Atypical interactions of integrin alphaVbeta8 with pro-TGF-beta1. *Proc. Natl. Acad. Sci. USA* **114**, E4168-E4174.

Xia, W. and Springer, T. A. (2014). Metal ion and ligand binding of integrin alpha5beta1. *Proc. Natl. Acad. Sci. USA* **111**, 17863-17868.

Xie, C., Shimaoka, M., Xiao, T., Schwab, P., Klickstein, L. B. and Springer, T. A. (2004). The integrin alpha-subunit leg extends at a Ca2+-dependent epitope in the thigh/genu interface upon activation. *Proc. Natl. Acad. Sci. USA* **101**, 15422-15427.

Xie, C., Zhu, J., Chen, X., Mi, L., Nishida, N. and Springer, T. A. (2010). Structure of an integrin with an alphaI domain, complement receptor type 4. *EMBO J.* **29**, 666-679.

Xiong, J.-P., Stehle, T., Diefenbach, B., Zhang, R., Dunker, R., Scott, D. L., Joachimiak, A., Goodman, S. L. and Arnaout, M. A. (2001). Crystal structure of the extracellular segment of integrin alpha Vbeta3. *Science* **294**, 339-345.

Xiong, J.-P., Stehle, T., Zhang, R., Joachimiak, A., Frech, M., Goodman, S. L. and Arnaout, M. A. (2002). Crystal structure of the extracellular segment of integrin alpha Vbeta3 in complex with an Arg-Gly-Asp ligand. *Science* **296**, 151-155.

Xu, X.-P., Kim, E., Swift, M., Smith, J. W., Volkmann, N. and Hanein, D. (2016). Three-dimensional structures of full-Length, membrane-embedded human alpha(IIb)beta(3) integrin complexes. *Biophys. J.* **110**, 798-809.

Ye, F., Hu, G., Taylor, D., Ratnikov, B., Bobkov, A. A., McLean, M. A., Sligar, S. G., Taylor, K. A. and Ginsberg, M. H. (2010). Recreation of the terminal events in physiological integrin activation. *J. Cell Biol.* **188**, 157-173.

Zhu, J., Luo, B.-H., Xiao, T., Zhang, C., Nishida, N. and Springer, T. A. (2008). Structure of a complete integrin ectodomain in a physiologic resting state and activation and deactivation by applied forces. *Mol. Cell* **32**, 849-861.